

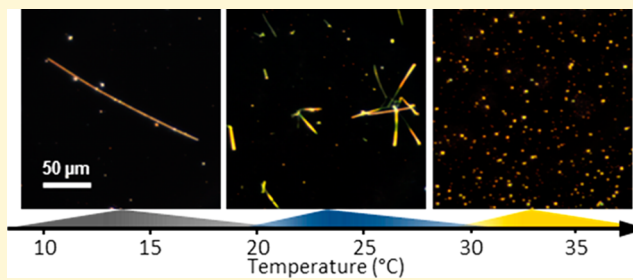
Synthesis and Crystal Structure of Gold Nanobelts

Courtney M. Payne,[†] Dmitri E. Tsentalovich,[‡] Denise N. Benoit,[†] Lindsey J. E. Anderson,[§] Wenhua Guo,^{||} Vicki L. Colvin,^{†,‡} Matteo Pasquali,^{†,‡} and Jason H. Hafner*,^{†,§}

[†]Department of Chemistry, [‡]Department of Chemical and Biomolecular Engineering, [§]Department of Physics and Astronomy, and ^{||}Smalley Institute for Nanoscale Science and Technology, Rice University, 6100 Main Street, Houston, Texas 77005, United States

Supporting Information

ABSTRACT: Gold nanobelts were synthesized by the reduction of tetrachloroauric acid with ascorbic acid in the presence of the surfactants cetyltrimethylammonium bromide and sodium dodecylsulfate. The resulting structures have rectangular cross sectional dimensions that are tens of nanometers and lengths that are tens to hundreds of micrometers. We find that the nanobelt yield and resulting structures are very sensitive to temperature which is likely due to the transition of the surfactant solution from wormlike micelles to spherical micelles. The nanobelt crystal structure contains a mixture of face centered cubic and hexagonally close packed lattice phases that can be isolated and examined individually due to the unique nanobelt size and shape.



INTRODUCTION

Gold nanobelts are elongated nanostructures that are many micrometers in length and have nanometer-scale rectangular cross sections. They exhibit sharp plasmon resonances that are tunable with their cross-sectional aspect ratio, defined as the nanobelt width divided by its height.^{1,2} Gold nanobelts also support propagating plasmon modes, thus acting as nanometer scale waveguides with high quantum confinement.³ Several strategies have been reported to synthesize both gold and silver nanobelts, but most are not as accessible as the widely practiced syntheses of gold nanospheres, nanorods, or other plasmonic nanoparticles. Gold and silver nanobelts have been grown in high temperature aqueous^{4,5} or organic solutions,^{6,7} by solid state methods,^{8,9} and by sonochemical and electrochemical reactions.^{10,11} However, the reaction yield is not always high^{6,12} and the resulting nanobelts can be defective.¹³

Aqueous room temperature synthesis of gold nanobelts has been achieved by reduction in surfactant solutions. Bakshi et al. prepared gold nanobelts with Gemini surfactant (14-2-14) using a seeded, multistep growth process.¹⁴ These nanobelts were found to grow at room temperature but not at 70 °C, leading the authors to conclude that belts are formed due to the soft template effect of the surfactant which is impeded at higher temperatures due to changes in surfactant phase. A second type of gold nanobelt was synthesized by Zhao et al. in a mixed surfactant solution containing cetyltrimethylammonium bromide (CTAB) and sodium dodecylsulfonate (SDS).¹⁵ Nanobelts were found to grow at two different temperatures leading to two distinct belt morphologies with unique crystallographic growth directions. By sampling the growth solution at various points in the synthesis, many nanobelts were found to grow and elongate out of central nuclei. Formation of gold nanobelts was attributed to the cooperative effect of the cationic-anionic

surfactant mixture as a binary capping agent. In both studies the resulting nanobelts were single crystalline, with heights less than 30 nm and widths less than 200 nm. While the effects of some synthetic parameters have been explored, the properties of the surfactant solutions and their underlying role in the nanobelt growth remain to be understood.

Previously, we have found that gold nanobelts grown in a mixture of CTAB and sodium dodecylsulfate (SDS) have peak plasmon resonant wavelengths ranging from 530 to 650 nm, proportional to a cross-sectional aspect ratio of 1 to 6.¹ We also observed a strong dependence on growth temperature, and we found several nanobelt morphologies, including highly uniform nanobelts, tapered nanobelts, and split nanobelts.² Here we provide some insights into the surfactant's role in the growth temperature dependence, as well as the crystalline morphology of the resulting gold nanobelts.

EXPERIMENTAL SECTION

Synthesis of Gold Nanobelts. CTAB, SDS, and tetrachloroauric(III) acid (HAuCl_4) were purchased from Sigma. L-ascorbic acid was purchased from Fisher. Gold nanobelts were typically synthesized as described previously.^{1,2} A mixture of CTAB and SDS was prepared by combining 650 μL of 50 mM CTAB and 500 μL of 10 mM SDS with 3.45 mL of room temperature HPLC grade water. Before mixing, both surfactant solutions were heated to a few degrees above room temperature to promote complete dissolution of the solid surfactant. After several seconds of gentle mixing, 100 μL of 10 mM HAuCl_4 was added. This solution was mixed by inversion several times and was then allowed to sit for 5 min. Finally, 300 μL of freshly prepared 100 mM L-ascorbic acid was added. The solution was then immediately

Received: July 24, 2013

Revised: December 17, 2013

Published: February 11, 2014



placed in a temperature controlled environment and left for 24 h. The resulting turbid solution contained a red precipitate that disperses into solution upon gentle mixing.

Sample Preparation. Several microliters of gold nanobelt solution were deposited onto a glass substrate and allowed to evaporate. The substrate was then viewed by dark field microscopy. TEM grids were prepared by the evaporation of several microliters of gold nanobelts onto lacey carbon grids (300 mesh), which were then gently rinsed with water.

Dynamic light scattering (DLS) and rheology experiments were performed using the surfactant mixture only. This solution was prepared by substituting the gold and ascorbic acid with water, keeping the surfactants at the same concentration as is used in the synthesis. Each of these experiments started at a low temperature and was heated to keep the conditions in the surfactant solution the same for each instrument. Analyzing the effect of the addition of the tetrachloroauric acid and ascorbic acid to the synthesis solution shows very little change in the solution pH. It is therefore likely that the micelle characteristics do not dramatically vary when only the CTAB and SDS components of the synthesis solution are present. For more details on this effect see Table S1 in the Supporting Information.

Characterization of Gold Nanobelts and Surfactant Solutions. Transmission electron microscopy (TEM) imaging and selected area electron diffraction (SAED) were performed using a JEOL JEM-2100F TEM operating at 200 kV with a double tilt holder (JEOL EM-316360). DLS measurements were taken using a Malvern Zetasizer Nano Zen 3600 equipped with a 633 nm laser. The effective micelle diameter was taken from the triplicate evaluation of the reported Z average. Shear rheology data was collected using a TA Instruments ARES equipped with a Neslab RTE-130 temperature control system. Dark field images were collected using epi-illumination dark field microscopy with a 50X/0.5 NA objective (Zeiss Axiovert 200M), a 100 W quartz tungsten halogen (QTH) light source, and Nikon DS500 camera.

RESULTS AND DISCUSSION

The surfactant based gold nanobelt synthesis yields nanobelts that are clearly visible and colorful in dark field microscopy due to plasmon resonant scattering. The nanobelt yield and structural details were highly dependent upon reaction temperature, as seen in Figure 1 (and Figure S1 in the Supporting Information for the complete temperature range examined). The gold nanobelt synthesis was performed at temperatures from 10 to 38 °C. Nanobelts synthesized at low temperature (below 22 °C) were isolated, nonbranched structures that often have a final length of several hundred micrometers. In contrast, growth from 22 to 30 °C gave substantially higher yields of nanobelt products with lengths of 10 to 30 μm. This midtemperature range produced both isolated nanobelts and others that were branched or clustered. The morphology of the nanobelts varies widely in this portion of the growth temperature range, yielding a variety of colors (530 to 650 nm) as well as nanobelts that taper along their length.² Above 30 °C nanobelt formation diminishes rapidly until, by 38 °C, only colloid is produced. The images in Figures 1 and S1 (Supporting Information) were taken with no sample processing (beyond deposition onto the glass slide) and represent the state of the nanobelts when viewed directly in the synthesis solution.

To gain greater insight into the synthetic mechanism, the nanobelt growth process was monitored in the microscope at room temperature (22 °C). A summary of the growth process is shown in Supporting Information Figure S2. Small, diffraction limited particles became visible within 45 min of reduction with ascorbic acid. Nanobelts were first observed about three hours later. These observations suggest that a two-

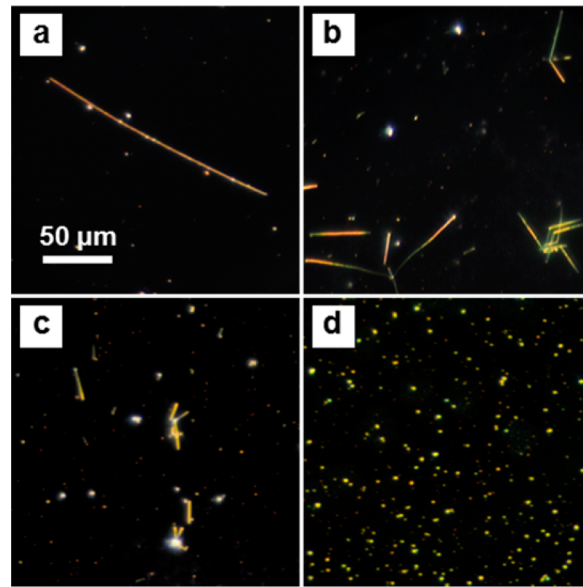


Figure 1. Dark field optical microscopy of gold nanobelts synthesized at (a) 18 °C, (b) 27 °C, (c) 32 °C, and (d) 35 °C. The 50 μm scale bar applies to all images. Parts a–c exhibit elongated nanobelts, while d only shows small colloidal gold particles.

step synthetic mechanism is likely, with a rapid initial formation of nuclei followed by a slower growth step in which the nanobelts elongate due to continued reduction of gold ions.

After the completion of the growth process, a common morphology of the midtemperature nanobelts is that of a branched “V” or tripod with a 120° angle between symmetric branches. The tripod geometry as shown in Figure 2a was frequently observed in the nanobelt synthesis product. In the TEM, small triangular nuclei (Figure 2b) as well as extended triangular structures (Figure 2c) were seen, suggesting that equilateral triangular structures are the nucleation sites for the nanobelts. The corners may be sites for rapid growth due to a specific interaction with the surfactants in a similar manner to gold nanorod and bipyramidal syntheses.^{16,17}

The gold nanobelt synthesis described here must be a complex process considering the varied nanobelt structures in Figures 1 and S1 (Supporting Information) that result from growth over a relatively small temperature range. In addition, we found that stirring the growth solution disrupted nanobelt formation. Even under slow stirring, only small gold particles were formed. This may indicate that the synthesis reaction is diffusion limited or that it is affected by rheological properties that are sensitive to solution conditions.

The characteristics of surfactant micelles have been well studied.¹⁸ Substantial research has gone into the properties of surfactant mixtures including the addition of salts, strongly binding counterions, and cosurfactants, as well as cationic and anionic surfactant mixtures.¹⁹ The role of the surfactant micelle in nanoparticle synthesis has previously been a subject of speculation, but it appears to be sensitive to the unique chemical conditions of each synthesis method.^{16,20} In an effort to explore how the cationic–anionic surfactant mixture influences the nanobelt synthesis, the surfactant micelles were characterized by DLS and shear rheology measurements.

The size of surfactant micelles in the CTAB/SDS mixture was estimated with DLS measurements for the temperature range of 20 to 35 °C, as shown in Figure 3. According to the

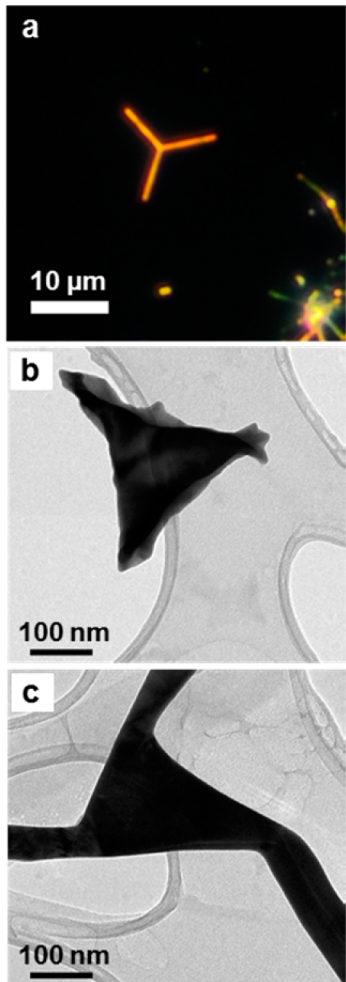


Figure 2. (a) Dark field optical image of a tripod shaped gold nanobelt. TEM of a (b) triangular nanobelt nucleus and (c) extended triangular nanobelt.

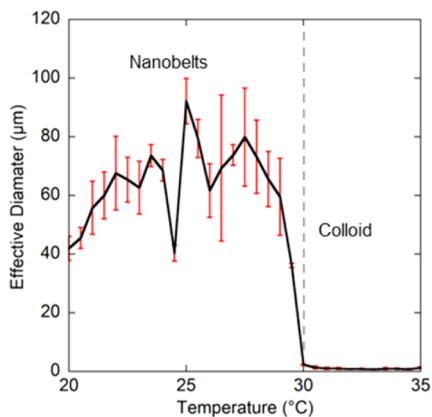


Figure 3. DLS measurements of the surfactant solution taken at temperatures ranging from 20 to 35 °C.

DLS data, the effective micelle size is large and remains relatively steady from 20 to 30 °C. Above 30 °C the micelle diameter drops dramatically, correlating to the approximate temperature where nanobelts no longer grow. This change suggests that nanobelt formation is related to micelle size, where larger micelles create nanobelts and smaller micelles produce only spherical colloid.

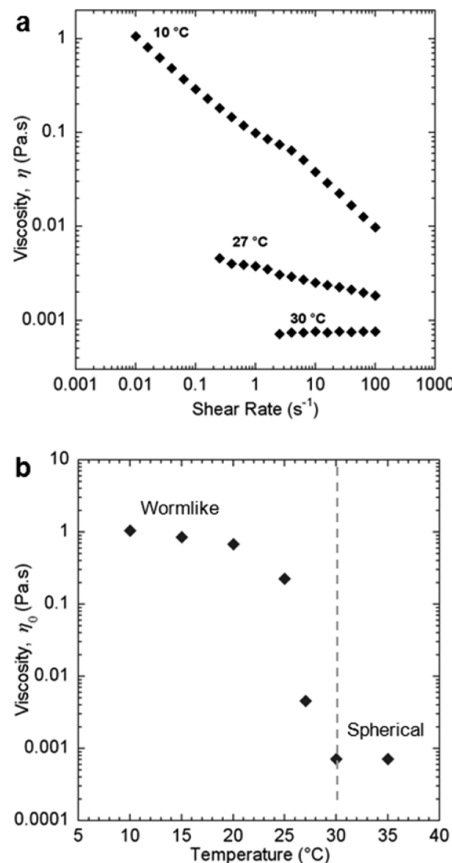
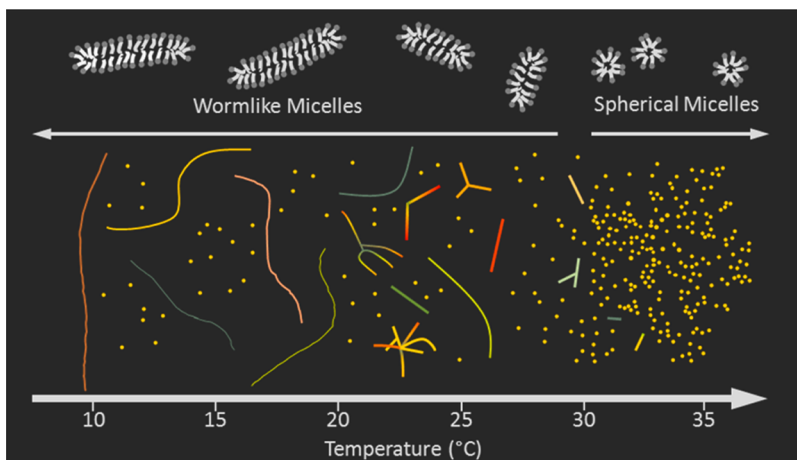


Figure 4. (a) Steady shear viscosity, η , of surfactant solution at three temperatures. (b) Zero-shear viscosity, η_0 , as a function of temperature.

The dependence of micelle conformation on temperature was further studied with steady shear rheology. Shear viscosity, η , of the surfactant mixture was measured as a function of shear rate for temperatures ranging from 10 to 35 °C (Figure 4a), allowing time for the solution to stabilize at each temperature. The strong shear-thinning behavior at temperatures below 20 °C resembles the rheological signature of solutions consisting of wormlike micelles.²¹ Above 20 °C, the shear thinning of the surfactant solution gets progressively weaker, until at 30 °C the solution starts to behave as a Newtonian fluid. The Newtonian behavior corresponds to the micelles adopting spherical morphologies.

The zero-shear viscosity, η_0 , taken to be the viscosity at the lowest shear rate accessible by the instrument, was plotted as a function of temperature (Figure 4b). Below 20 °C, η_0 remains around 1.0 Pa·s, correlating to the region in which low temperature nanobelts grow. Between 20 and 30 °C, η_0 decreases rapidly before leveling off above 30 °C at around 7.1×10^{-4} Pa·s (essentially the viscosity of water at that temperature). In this temperature range, the nanobelts tend to be shorter and more complex in structure. The viscosity of water over that same temperature range only changes from 1.3×10^{-3} Pa·s to 7.2×10^{-4} Pa·s compared to the 3 orders of magnitude change that is seen in the surfactant solution.²²

Rheological studies of similar cationic-anionic surfactant mixtures have revealed that the zero shear viscosity is strongly affected by the relative ratios of surfactant mixtures; supporting measurements by neutron scattering and cryo-TEM have shown that the increased viscosity is due to the formation of

Scheme 1. Depiction of the Correspondence between the Micelle Structure and Nanobelt Product^a

^aWith increasing temperature, the surfactant transitions from wormlike micelles (much longer than depicted) to spherical micelles, and the nanobelts transition from long isolated wires to shorter branched structures and spherical nanoparticles.

networks of branched wormlike micelles.^{23–26} Micelle elongation to wormlike structures occurs in cationic–anionic surfactant mixtures because of the charge neutralization of the micelle surface potential.¹⁹ A related study by Davies et al. of a solution of CTAB and 5-methylsalicylic acid showed that varying the relative surfactant concentration produced similar results as changing the temperature of the solution.²² Dramatic changes in zero shear viscosity and the transition from shear thinning to Newtonian behavior of the CTAB and 5-methylsalicylic acid mixture were correlated with the transition from wormlike to spherical micelles, as seen in previous studies.²¹

The DLS and rheological measurements reveal a clear link between the shape of the nanobelts and the structure of the surfactant assemblies, as summarized in Scheme 1. With increasing temperature from 10 to 35 °C, the nanobelts transition from very long isolated structures, to shorter branched structures, to spherical nanoparticles. On the basis of the large effective DLS size and shear rheology measurements the CTAB/SDS surfactant mixture also transitions from long wormlike micelles to small spherical micelles. This similarity suggests that the elongated structures of wormlike micelles act in some way as soft templates for nanobelt growth.

To separate the role that the micelles play as a template for nanobelt growth from the increase in viscosity that arises from the micelle network (related to a diffusion based growth mechanism), gold nanobelts were synthesized at 27 °C, in the region where the nanobelts are shorter and branched, but with the addition of PEG (MW = 8000 g/mol, added at 0, 5, 10, and 20 wt % of the final solution) as a thickening agent²⁷ to increase the solution's viscosity and lower the ion diffusivity. If the nanobelt elongation mechanism were diffusion-limited, the increased solution viscosity would yield nanobelts similar to the long isolated nanobelts seen at lower temperatures (such as those in Figure 1a), rather than the typical shorter branched belts seen at 27 °C (Figure 1b). Instead, all four solutions yielded branched, varied nanobelts, with nanobelt length and quality gradually decreasing with increasing PEG concentration, as seen in Supporting Information Figure S3. This indicates that the wormlike micelles do not simply increase viscosity but that the actual micelle morphology must play a role in the synthesis. This conclusion is also supported by the failure of the

nanobelt synthesis upon stirring, since the stirring motion disrupts the wormlike micelle network, as seen in the shear rheology data.²⁸

The crystal structure of the final nanobelt product was also examined. TEM and SAED of a nanobelt synthesized at 27 °C are shown in Figure 5a and 5b. SAED shows the [111] FCC zone of the {220} planes that is observed for bulk gold. Additionally, there is a second set of weak reflections that correspond to the [0001] HCP zone of the {10̄10} planes.²⁹ This pattern has been observed before in thin, atomically flat gold and silver structures and is often referred to as the 1/3{422} FCC forbidden planes.^{30–34} It has been theorized that these planes arise from stacking faults within the crystal or from surface reorganization.²⁹

To better conceptualize how these two phases occur in the nanobelts, high resolution TEM (HRTEM) was taken of the belt shown in Figure 5a and fast Fourier transform (FFT) was taken of this image (Figure 5c,d) using Gatan DigitalMicrograph software. By masking each independent region in the FFT of the high resolution image the FCC (Figure 5e) structure can be separated from that of the HCP (Figure 5f). When the inverse FFT of these masked areas is performed, the clarity of the resulting images demonstrates the contribution of each lattice phase to the overall nanobelt structure. The FCC phase is found uniformly distributed throughout the nanobelt (Figure 5g), while the HCP phase (Figure 5h) has varying contrast, which indicates uneven HCP presence throughout the structure. Because the two phases are in the same zone, it can be inferred that domains of HCP exist in a predominantly FCC lattice, rather than a uniform series of stacking faults. These domains can be visualized directly in Figure 5g,h. The lattice spacing calculated from the inverse FFT is 0.148 and 0.253 nm for the FCC and HCP phases, respectively. HCP gold structures are of particular interest due to the potential for new physical properties. This topic has been recently investigated by thin HCP gold sheets grown on graphene oxide.^{35,36} Gold nanobelts are a unique platform to study this lattice mixture due to the mesoscopic nature of their thin, flat, and extended structure, which may be a product of the complex growth mechanism.

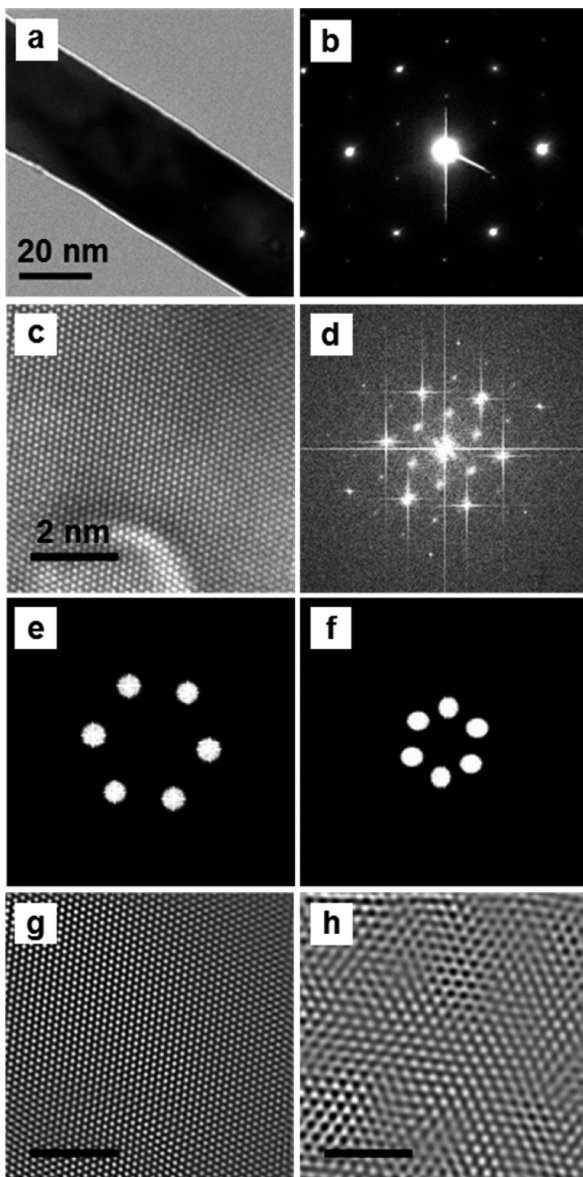


Figure 5. (a) TEM and (b) SAED (showing both the FCC and HCP reflections) and (c) HRTEM of a 27 °C gold nanobelt. The (d) FFT of the HRTEM image shows two distinct patterns. These can be masked to show only the (e) FCC and (f) HCP sections. The inverse FFT of the masked areas (at the same scale as (c)) gives the individual contribution of the (g) FCC and (h) HCP lattice character.

CONCLUSIONS

Here we have investigated the growth mechanism of gold nanobelts under mild aqueous conditions in mixed surfactants. The nanobelt shape and yield vary considerably over a narrow temperature range. It appears that the growth mechanism is a two-step process, with a rapid seed formation step, followed by a slower nanobelt growth stage. The morphology of the final nanobelt product is influenced by the structure of the surfactant mixture. The networks of micelles in the growth solution change dramatically with temperature in a manner that corresponds to the different nanobelt growth regions. Additionally, when the nanobelt crystal structure is examined, two distinct lattice phases appear to be present. Within the predominantly FCC lattice, we have detected distinct domains

of the HCP phase which can be characterized by the isolation of the two patterns visible in the FFT of the HRTEM image.

ASSOCIATED CONTENT

Supporting Information

Additional table and figures. This material is available free of charge via the Internet at <http://pubs.acs.org>.

AUTHOR INFORMATION

Corresponding Author

*(J.H.H.) E-mail: hafner@rice.edu.

Notes

The authors declare no competing financial interest.

ACKNOWLEDGMENTS

The authors acknowledge support from the National Science Foundation under Grant 1037575 (J.H.H., C.M.P.) and the Robert A. Welch Foundation under Grants C-1761 (J.H.H., C.M.P., L.J.E.A.) and C-1668 (M.P.). Additionally, this work was supported by a training fellowship from the Keck Center Nanobiology Training Program of the Gulf Coast Consortia (NIH Grant T32EB009379) (V.L.C., D.N.B.) and Center for Biological and Environmental Nanotechnology Grant EEC-0647452 (V.L.C., D.N.B.).

REFERENCES

- (1) Anderson, L. J. E.; Payne, C. M.; Zhen, Y.-R.; Nordlander, P.; Hafner, J. H. *Nano Lett.* **2011**, *11* (11), 5034–5037.
- (2) Payne, C. M.; Anderson, L. J. E.; Hafner, J. H. *J. Phys. Chem. C* **2013**, *117* (9), 4734–4739.
- (3) Anderson, L. J. E.; Zhen, Y.-R.; Payne, C. M.; Nordlander, P.; Hafner, J. H. *Nano Lett.* **2013**, *13* (12), 6256–6261.
- (4) Yang, Z. Q.; Nguyen, K. T.; Chen, H. Y.; Qian, H. J.; Fernando, L. P.; Christensen, K. A.; Anker, J. N. *J. Phys. Chem. Lett.* **2011**, *2* (14), 1742–1746.
- (5) Zhang, J. H.; Liu, H. Y.; Wang, Z. L.; Ming, N. B. *Appl. Phys. Lett.* **2007**, *91* (13), 133112.
- (6) Sun, Y. G.; Mayers, B.; Xia, Y. N. *Nano Lett.* **2003**, *3* (5), 675–679.
- (7) He, X.; Zhao, X. J.; Li, Y. Z.; Sui, X. T. *J. Mater. Res.* **2009**, *24* (7), 2200–2209.
- (8) Chen, Y.; Somsen, C.; Milenkovic, S.; Hassel, A. W. *J. Mater. Chem.* **2009**, *19* (7), 924–927.
- (9) Chen, Y.; Milenkovic, S.; Hassel, A. W. *Nano Lett.* **2008**, *8* (2), 737–742.
- (10) Zhang, J. L.; Du, J. M.; Han, B. X.; Liu, Z. M.; Jiang, T.; Zhang, Z. F. *Angew. Chem., Int. Ed.* **2006**, *45* (7), 1116–1119.
- (11) Liu, B. Q.; Luo, W.; Zhao, X. P. *Mater. Res. Bull.* **2009**, *44* (3), 682–687.
- (12) Song, Y. Z.; Dong, J. M.; Liu, B.; Wang, Y. F.; Li, X. D.; Liu, G. H. *Rare Metal Mater. Eng.* **2010**, *39* (4), 711–714.
- (13) Huang, L.; Zhang, Y.; Guo, Z. R.; Gu, N. *Chin. Sci. Bull.* **2009**, *54* (9), 1626–1629.
- (14) Bakshi, M. S.; Possmayer, F.; Petersen, N. O. *J. Phys. Chem. C* **2008**, *112* (22), 8259–8265.
- (15) Zhao, N.; Wei, Y.; Sun, N. J.; Chen, Q. J.; Bai, J. W.; Zhou, L. P.; Qin, Y.; Li, M. X.; Qi, L. M. *Langmuir* **2008**, *24* (3), 991–998.
- (16) Orendorff, C. J.; Murphy, C. J. *J. Phys. Chem. B* **2006**, *110* (9), 3990–3994.
- (17) Liu, M. Z.; Guyot-Sionnest, P. *J. Phys. Chem. B* **2005**, *109* (47), 22192–22200.
- (18) Larson, R. G. *The Structure and Rheology of Complex Fluids*; OUP: 1999.
- (19) Berret, J. *Rheology of Wormlike Micelles: Equilibrium Properties and Shear Banding Transitions*. In *Molecular Gels: Materials*

- with *Self-assembled Fibrillar Networks*; Weiss, R. G., Terech, P., Eds.; Springer: London: 2006; pp 667–720.
- (20) Nikoobakht, B.; El-Sayed, M. A. *Chem. Mater.* **2003**, *15* (10), 1957–1962.
- (21) Davies, T. S.; Ketner, A. M.; Raghavan, S. R. *J. Am. Chem. Soc.* **2006**, *128* (20), 6669–6675.
- (22) Kestin, J.; Sokolov, M.; Wakeham, W. A. *J. Phys. Chem. Ref. Data* **1978**, *7* (3), 941–948.
- (23) Koehler, R. D.; Raghavan, S. R.; Kaler, E. W. *J. Phys. Chem. B* **2000**, *104* (47), 11035–11044.
- (24) Koshy, P.; Aswal, V. K.; Venkatesh, M.; Hassan, P. A. *J. Phys. Chem. B* **2011**, *115* (37), 10817–10825.
- (25) Raghavan, S. R.; Fritz, G.; Kaler, E. W. *Langmuir* **2002**, *18* (10), 3797–3803.
- (26) Lin, Z.; Cai, J. J.; Scriven, L. E.; Davis, H. T. *J. Phys. Chem.* **1994**, *98* (23), 5984–5993.
- (27) Gonzalez-Tello, P.; Camacho, F.; Blazquez, G. *J. Chem. Eng. Data* **1994**, *39* (3), 611–614.
- (28) Jain, S.; Bates, F. S. *Science* **2003**, *300*, 460–464.
- (29) Kirkland, A. I.; Edwards, P. P.; Jefferson, D. A.; Duff, D. G. Chapter 8. The structure, characterization, and evolution of colloidal metals. In *Annual Reports on the Progress of Chemistry Section "C" (Physical Chemistry)*; The Royal Society of Chemistry: 1990; Vol. 87, pp 247–304.
- (30) Jin, R.; Cao, Y.; Mirkin, C. A.; Kelly, K. L.; Schatz, G. C.; Zheng, J. G. *Science* **2001**, *294* (5548), 1901–1903.
- (31) Liang, H. Y.; Yang, H. X.; Wang, W. Z.; Li, J. Q.; Xu, H. X. *J. Am. Chem. Soc.* **2009**, *131* (17), 6068–6069.
- (32) Shen, X. S.; Wang, G. Z.; Hong, X.; Xie, X.; Zhu, W.; Li, D. P. *J. Am. Chem. Soc.* **2009**, *131* (31), 10812–10813.
- (33) Lim, B.; Camargo, P. H. C.; Xia, Y. N. *Langmuir* **2008**, *24* (18), 10437–10442.
- (34) Kan, C. X.; Zhu, X. G.; Wang, G. H. *J. Phys. Chem. B* **2006**, *110* (10), 4651–4656.
- (35) Huang, X.; Li, H.; Li, S. Z.; Wu, S. X.; Boey, F.; Ma, J.; Zhang, H. *Angew. Chem., Int. Ed.* **2011**, *50* (51), 12245–12248.
- (36) Huang, X.; Li, S. Z.; Huang, Y. Z.; Wu, S. X.; Zhou, X. Z.; Gan, C. L.; Boey, F.; Mirkin, C. A.; Zhang, H. *Nat. Commun.* **2011**, *2*, Article number 292.